Monte Carlo simulations of a simple model for the electrocatalytic CO oxidation on platinum

Monte Carlo simulations of a simple model for the electrocatalytic CO oxidation on platinum

M. T. M. Koper, A. P. J. Jansen, and R. A. van Santen
Laboratory of Inorganic Chemistry and Catalysis, Eindhoven University of Technology, 5600 MB Eindhoven, The Netherlands

J. J. Lukkien and P. A. J. Hilbers
Department of Mathematics and Computing Science, Eindhoven University of Technology, 5600 MB Eindhoven, The Netherlands

(Received 3 April 1998; accepted 9 July 1998)

A simple lattice-gas model for the electrocatalytic carbon monoxide oxidation on a platinum electrode is studied by dynamic Monte Carlo simulations. The CO oxidation takes place through a Langmuir–Hinshelwood reaction between adsorbed CO and an adsorbed OH radical resulting from the dissociative adsorption of water. The model enables the investigation of the role of CO surface mobility on the macroscopic electrochemical response such as linear sweep voltammetry and potential step chronoamperometry. Our results show that the mean-field approximation, the traditional but often tacitly made assumption in electrochemistry, breaks down severely in the limit of vanishing CO surface mobility. Comparison of the simulated and experimental voltammetry suggests that on platinum CO oxidation is the intrinsically fastest reaction on the surface and that CO has a high surface mobility. However, under the same conditions, the model predicts some interesting deviations from the potential step current transients derived from the classical nucleation and growth theories. Such deviations have not been reported experimentally. Furthermore, it is shown that our simple model predicts different Tafel slopes at low and high potential, the qualitative features of which are not strongly influenced by the CO mobility. The comparison of our simulation results to the experimental literature is discussed in some detail. © *1998 American Institute of Physics.* [S0021-9606(98)70738-X]

I. INTRODUCTION

The electrocatalytic oxidation of carbon monoxide on a platinum electrode is one of the most intensively studied systems in electrocatalysis.[1–15] The understanding of the adsorption and electrochemical oxidation of poisonous CO is of paramount importance in the development of improved low temperature fuel cells. Furthermore, CO is a relatively simple molecule which is ideally suited for model studies of molecular adsorption at the metal/electrolyte interface, and its oxidation mechanism is believed to be a simple Langmuir–Hinshelwood surface reaction. *In situ* electrochemical measurements such as STM and FTIR,[14] as well as information obtained on emersed electrodes in UHV,[6,11] has yielded a wealth of structural data on CO adsorption on platinum single-crystal electrodes. However, it has remained relatively unclear how these microscopic structural features, or more generally the distribution of adsorbed CO on the electrocatalyst surface, affect the overall macroscopic electrocatalytic activity. Questions like what role is played by the surface migration of CO and the possible formation of islands during the oxidation are not easily resolved by such essentially static methods.

In this paper we want to address these questions theoretically by studying a simple reaction model for the CO oxidation on a Pt(100) electrode using Monte Carlo (MC) simulations. In theoretical treatments of the electrochemical response of electrocatalytic systems, such as linear sweep and cyclic voltammetry, the analysis is usually based on macroscopic reaction-rate or isotherm equations derived from the so-called mean-field approximation. The Monte Carlo technique offers the possibility to calculate the exact electrochemical response for the reaction model under study, without any further approximation introduced in the statistical mechanics. Monte Carlo methods have already been used in surface electrochemistry to describe the (competitive) adsorption of ions at single-crystal electrodes.[16–18] However, no extensive use has yet been made of dynamic Monte Carlo simulations in electrochemistry (but see Refs. 17–19), and there has not yet appeared a Monte Carlo study of cyclic voltammetry including the correct time dependence of the rate constants. By a special method which allows the introduction of time-dependent reaction rate constants in the Monte Carlo algorithm in a computationally efficient and exact way,[20] we can obtain cyclic voltammograms and chronoamperometric transients on relatively large lattices in a limited amount of computer time. Since CO oxidation has been modeled extensively at the Pt/gas interface,[21] it also seems a good starting point for the modeling of electrocatalytic phenomena at the Pt/solution interface.

The model we study is a simple ''A+B'' reaction on a square lattice. Although such a model is certainly not sufficiently realistic if one aims at understanding the detailed structural features of CO adsorption at the metal/electrolyte interface, we believe that as far as the macroscopic electrochemical response of the CO oxidation is concerned, our model is able to provide some interesting new insights into

the importance of microscopic features such as mixing, lateral diffusion, and island formation. These results certainly have relevance to CO oxidation, but clearly also to any other electrochemical ''A+B'' reaction.

The paper is organized as follows. In Sec. II, we give the reaction model for CO oxidation on Pt(100), as well as the system's equations based on the mean-field approximation. Next we discuss briefly how our MC method solves the master equation describing the configurational changes on the lattice with the correct time dependence, and in particular how it deals with the time dependence of the rate constants in a linear sweep or cyclic voltammetry experiment. The results of extensive simulations of the voltammetry and chronoamperometric potential-step transients are presented in Sec. III. The simulations will be compared to the mean-field predictions, to the classical nucleation-and-growth theory, and to experiment, aiming to assess the importance of lateral CO diffusion on the electrocatalytic performance of the surface. Section IV summarizes our main results and discusses the possibilities for future theoretical and experimental work.

II. THEORY AND COMPUTATIONAL METHODS

A. The reaction model

As early as 1964, Gilman[1] proposed that the electrochemical CO oxidation in acidic solution involves a surface reaction between adsorbed CO molecules and an adsorbed oxygen-containing species. The exact nature of this latter species, the two most likely candidates being adsorbed water and adsorbed hydroxyl, is still somewhat controversial. As electrochemical measurements indicate that both the formation of the oxygen-containing species and the CO oxidation reaction are potential dependent, we will adhere to the most commonly accepted view that it is an adsorbed OH species resulting from the dissociative water oxidation. In acidic solution, the reaction model is:

$$H_2O + * \rightleftharpoons OH_{ads} + H^+ + e^-, \tag{2.1}$$

$$CO_{ads} + OH_{ads} \rightarrow CO_2 + H^+ + e^- + 2*, \tag{2.2}$$

with ''*'' denoting a free surface site. (More realistically, an empty site would correspond to a physisorbed water molecule.) For simplicity, both species are assumed to compete for the same on-top sites on a square lattice. It is known that for high CO coverages the most dominant binding site for CO is the on-top site.[8] The adsorption site for OH on transition-metal surfaces is controversial and presumably depends on the lateral adsorbate interactions;[22] in *ab initio* quantum-chemical calculations, the preferred adsorption site on small Pt clusters is found to be the one-fold on-top site.[23] From *in-situ* IR and STM measurements, at high CO coverages some CO is known to be adsorbed on the bridge-bonded and multicoordinated sites.[8,14] The oxidation of the latter gives rise to a small prewave in the voltammetric curve on Pt(111). Clearly our model will not be able to reproduce such a prewave.

In our model, the reaction between CO and OH can only take place if they occupy neighboring sites. The rate constants of the reactions are assumed to obey the Butler–Volmer law for electrochemical reactions,[28] and are given by

TABLE I. Rate constants.

Process	Rate constant	FAST	SLOW
OH adsorption	k_1^0	0.02	0.02
OH desorption	k_{-1}^0	10^4	10^4
CO oxidation	k_2^0	0.8234	8.234×10^{-5}

$$k_{OH,ads} = k_1 = k_1^0 \exp(\alpha_1 e_0 E/k_B T), \tag{2.3}$$

$$k_{OH,des} = k_{-1} = k_{-1}^0 \exp(-(1-\alpha_1) e_0 E/k_B T), \tag{2.4}$$

$$k_{CO_2,des} = k_2 = k_2^0 \exp(\alpha_2 e_0 E/k_B T), \tag{2.5}$$

where the α's are the transfer coefficients (taken 0.5 in all that follows), E is the electrode potential, and e_0, k_B, and T have their usual meaning. In the following, the subscripts ''1,'' ''−1,'' and ''2'' refer to the OH adsorption, OH desorption and the CO oxidation reactions, respectively. The rate constants k_1^0 and k_{-1}^0 include the water and proton concentrations at the surface, respectively, which are both assumed to be constant. The reaction rate constants all have the dimension s^{-1}. The total current density due to these reactions is given by Faraday's law

$$i = e_0(v_1 - v_{-1} + v_2), \tag{2.6}$$

where v_j denotes the rate of the jth reaction (in $cm^{-2}\ s^{-1}$). The mean-field expressions for these reaction rates are given by

$$v_1 = \Gamma_s k_1 (1 - \theta_{OH} - \theta_{CO}), \tag{2.7}$$

$$v_{-1} = \Gamma_s k_{-1} \theta_{OH}, \tag{2.8}$$

$$v_2 = \Gamma_s Z k_2 \theta_{CO} \theta_{OH}, \tag{2.9}$$

where Γ_s is the number of surface sites per cm^2 ($\approx 1.32\times10^{15}$ for a Pt(100) surface), and $Z=4$ (the number of nearest neighbors on a square lattice).

The time evolution of the average coverages θ_{CO} and θ_{OH} is given by the differential equations,

$$\Gamma_s \frac{d\theta_{OH}}{dt} = v_1 - v_{-1} - v_2, \tag{2.10}$$

$$\Gamma_s \frac{d\theta_{CO}}{dt} = -v_2. \tag{2.11}$$

To calculate a linear sweep or cyclic voltammogram, the equations are solved by specifying a certain initial condition (usually $\theta_{CO}(t=0) = \theta_{CO}^i$ and $\theta_{OH}(t=0) = 0$) and a certain potential sweep program $E(t) = E_i + vt$, with E_i the starting potential and v the sweep rate, using standard numerical integration techniques.

We consider the oxidation of a certain (submonolayer) amount of CO preadsorbed onto the surface, with no CO present in the solution. Experimental saturation coverages for CO on Pt correspond to ~0.7 CO per Pt site.[12] In our simulations, a coverage of 0.99 is considered as a saturation coverage. We use two different sets of rate constants, which are given in Table I. The rate constants for OH adsorption and desorption were chosen such that for 50 mV s^{-1} the OH adsorption appears quite reversible. In the FAST set of rate

constants, the CO+OH oxidation reaction is assumed to be (much) faster than the OH adsorption reaction; in the SLOW set of rate constants, the CO+OH oxidation reaction is assumed to be (much) slower than the OH adsorption. The two sets enable us to make a *qualitative* comparison of the different electrochemical responses of FAST and SLOW. Hence the potential axis we use is to some extent arbitrary. As we will argue in Sec. III E, FAST seems qualitatively similar to the CO oxidation on Pt(100), whereas SLOW shows similarities with the CO oxidation on Rh(100). In the MC simulation, we also have to specify the rate of CO surface diffusion, i.e., the rate of CO exchanging places with an empty neighboring site (or with a physisorbed water molecule),

$$CO_{ads} + * \rightarrow * + CO_{ads}. \tag{2.12}$$

This ''reaction'' has a rate of $D\ s^{-1}$, corresponding to a surface diffusion coefficient of $\sim 10^{-15} \times D\ cm^2\ s^{-1}$. At the Pt/vacuum interface, D lies in the range $10^{-9}-10^{-11}\ cm^2\ s^{-1}$ at room temperature.[29] At the Pt/water interface, no quantitative estimate of D is known, but one may expect it to be lower than at the Pt/vacuum interface as CO will have to displace physisorbed water molecules. Hence, in our simulations the parameter D is varied within the two sets of rate constants in order to assess the influence of CO surface diffusion on the overall electrochemical response. Diffusion of OH is not considered in our MC simulations, unless stated otherwise. Note that in our model the rate and diffusion constants implicitly incorporate the role of the interfacial solvation, as the detailed solvent structure at the Pt/solution interface is not considered in our simulation.

B. Monte Carlo method for solving the master equation with time-dependent reaction rates

For completeness, we summarize the main principles of the dynamical Monte Carlo method for solving the master equation with time-dependent reaction rate constants. Details of the method have been published elsewhere.[20] Expressions for the particular time dependence that we used in our simulations are given explicitly, as these have some theoretical significance.

The master equation can be written as

$$\frac{dP_\beta}{dt} = \sum_{\beta'} [W_{\beta' \rightarrow \beta} P_{\beta'} - W_{\beta \rightarrow \beta'} P_\beta]. \tag{2.13}$$

Here β and β' denote configurations of the adlayer, and P_β and $P_{\beta'}$ the probability of their occurrence. The master equation describes how this probability changes with time due to the surface reactions. These reactions have rate constants; $W_{\beta' \rightarrow \beta}$ is the rate constant of the reaction that changes configuration β' into β. An efficient Monte Carlo method to solve this master equation with time-dependent rate constants is the First Reaction Method. Suppose that at time t the system is in configuration β. For each reaction $\beta \rightarrow \beta'$ the master equation gives us a probability distribution for the time that this reaction will occur. A time step $\Delta t_{\beta \rightarrow \beta'}$ is picked from each distribution. The reaction with the smallest Δt occurs first. The configuration is changed accordingly, and the time is incremented. This procedure is repeated until certain preset conditions are met (e.g., until the final potential of a linear sweep is reached).

All possible transitions $\beta \rightarrow \beta'$ can be classified into four categories, cf. reactions (2.1), (2.2), and (2.12). Hence there are only four distinct values for the transition rate $W_{\beta \rightarrow \beta'}$, namely k_1, k_{-1}, k_2, and D. The general expression for k_i is according to the Butler–Volmer law

$$k_i = k_i^0 \exp\left[\frac{\alpha e_0 E}{k_B T}\right]. \tag{2.14}$$

The probability $P(\tau)$ that this transition has not yet occurred after a time τ is then

$$P(\tau) = \exp\left[-\int_t^{t+\tau} dt' k_i(t')\right], \tag{2.15}$$

where the time dependence of k_i is through the time dependence of the electrode potential E. With

$$E(t+\tau) = E(t) + v\tau \tag{2.16}$$

the integral can be solved explicitly, yielding

$$P(\tau) = \exp\left[\frac{-k_i^0 k_B T}{\alpha e_0 v} \exp\left(\frac{\alpha e_0 E(t)}{k_B T}\right)\left\{\exp\left(\frac{\alpha e_0 v \tau}{k_B T}\right) - 1\right\}\right]. \tag{2.17}$$

The time interval after which the reaction occurs is then given by the solution of the equation

$$P(\tau) = r, \tag{2.18}$$

where r is a random deviate of the unit interval. A remarkable property of Eq. (2.17) is that if $\alpha v < 0$ (i.e., the activation energy increases with time, such as occurs for a reduction reaction under a positive-going voltage ramp) there is a finite probability that $P(\tau)$ does not go to zero when $\tau \rightarrow \infty$, but rather to

$$\lim_{\tau \rightarrow \infty} P(\tau) = \exp\left[\frac{k_i^0 k_B T}{\alpha e_0 v} \exp\left(\frac{\alpha e_0 E(t)}{k_B T}\right)\right]. \tag{2.19}$$

This means that there is a finite probability that the reaction will not occur at all. As a consequence, Monte Carlo methods that are based on average reaction types, instead of Eq. (2.18), cannot be used, because such averages cannot be defined.[24]

C. CARLOS

The method described above was implemented in the CARLOS program, described in detail in Ref. 25. This is a general-purpose program for dynamic Monte Carlo simulations of surface reactions. It also contains the Variable Step Method and the Random Selection Method, two methods that are preferable for simulating systems with rate constants that do not vary with time. A more complex reaction system for which these methods have been used can be found in Ref. 26.

The simulations were performed on either a 128×128 or a 256×256 square lattice with periodic boundary conditions. Apart from a lower noise level on the larger lattice, we did not observe any difference between the two lattices. All vol-

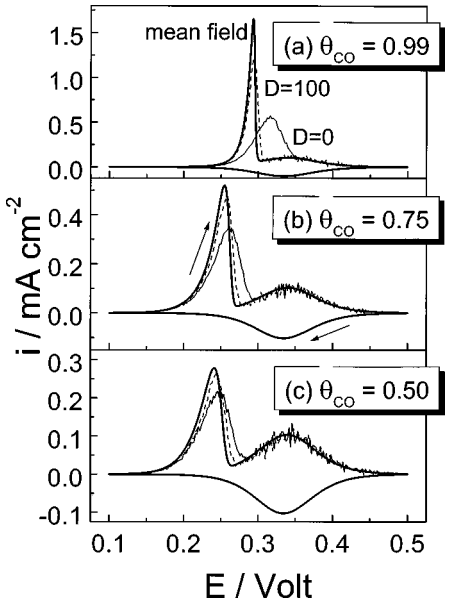

FIG. 1. Cyclic voltammograms for the FAST set of rate constants at three different initial coverages of CO, as indicated in the figure. Sweep rate 50 mV s^{-1}. Thick solid line, mean field; thin dashed line, $D=100$; thin solid line, $D=0$.

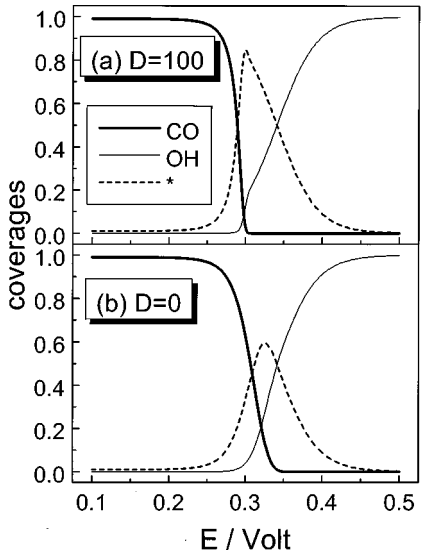

FIG. 2. CO, OH and * coverages during the voltammetric sweeps of Fig. 1(a).

tammograms and potential step transients to be presented below were carried out on the larger lattice size. Snapshots show the 128×128 lattice. The temperature was fixed at 300 K.

III. RESULTS AND DISCUSSION

A. Cyclic voltammetry of FAST

In Fig. 1 we show the three cyclic voltammograms (at 50 mV s^{-1}) for stripping off oxidatively $\theta^{i}_{CO}=$ 0.99, 0.75 and 0.50 submonolayers of preadsorbed CO for three different CO diffusion rates. The rates constants are those from the

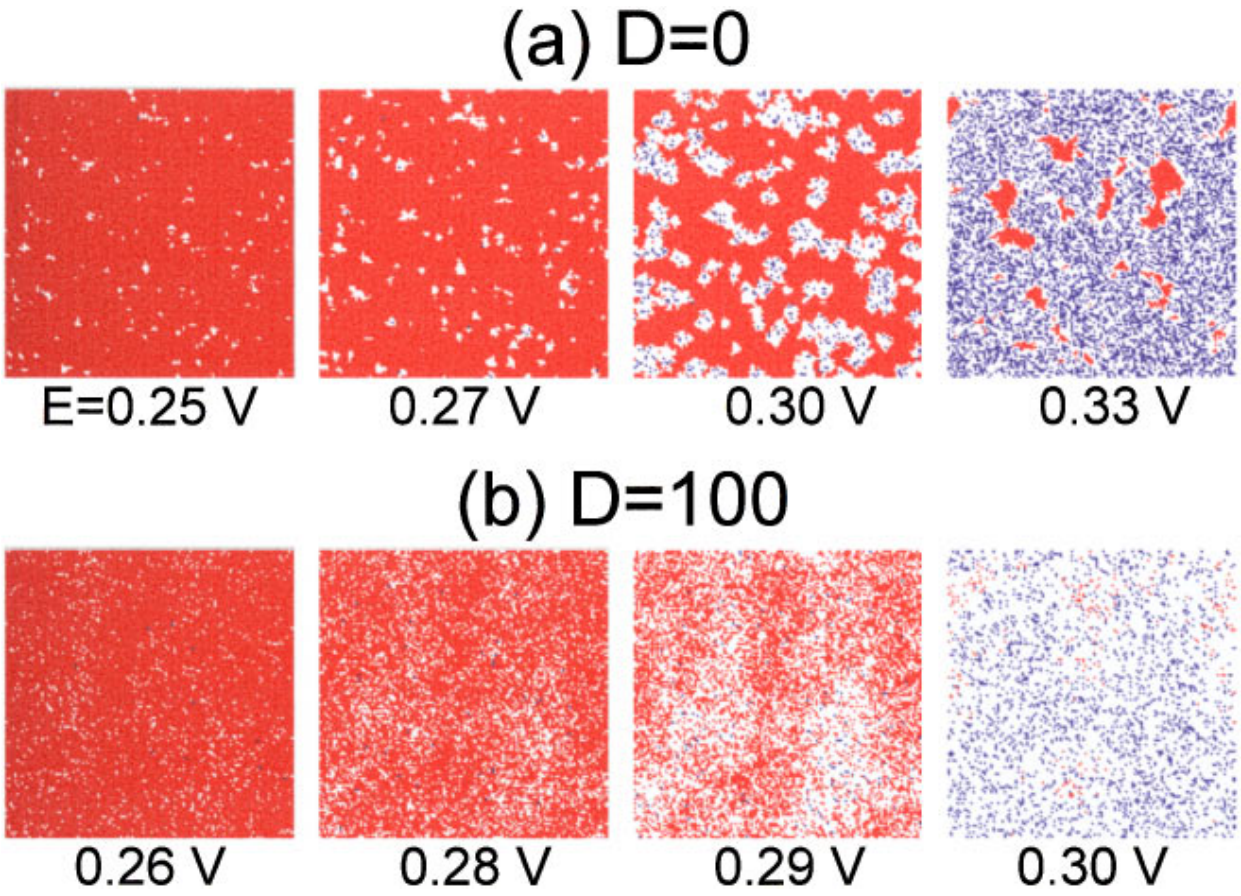

FIG. 3. Snapshots of the electrode surface during the voltammograms of Fig. 1(a). Blue, OH; Red, CO; White, empty site.

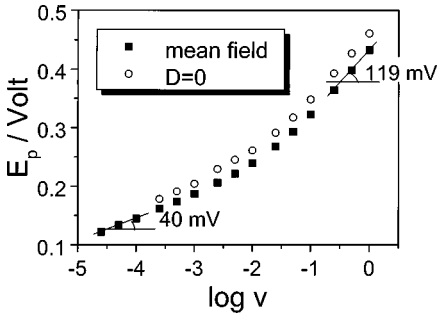

FIG. 4. Peak potential E_p as a function of the logarithm of the sweep rate v.

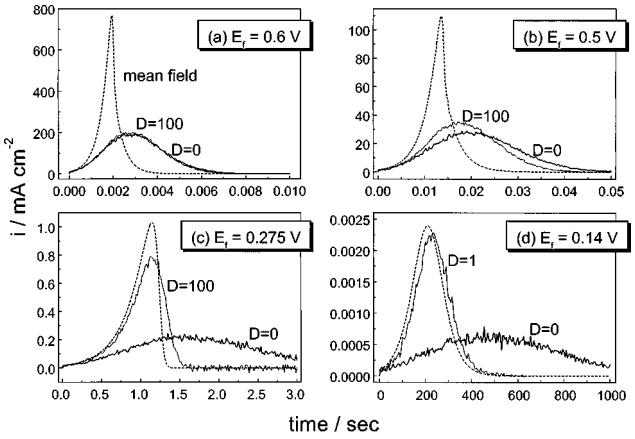

FIG. 5. Potential step current transients for the FAST set of rate constants from a 0.99 CO monolayer to four different final potentials E_f, as indicated in the figure. Note that time and current axes are different for all four potentials.

FAST column of Table I. In all three cases, the initial configuration was a random configuration created by the CARLOS program. The difference between the mean-field voltammetry ($D=\infty$) and the $D=0$ voltammetry is the largest for high initial coverage [$\theta_{\mathrm{CO}}^{i}=0.99$ in Fig. 1(a)]. As OH has to adsorb in the ''holes'' in the CO layer, there are large regions of CO that can be oxidized only at the perimeter of the existing holes. If CO diffuses, these holes effectively diffuse and the OH adsorption can take place at many different places, making more CO available for attack by OH. Furthermore, CO can diffuse towards OH already present on the surface and react. Both mechanisms enhance the mixing and suppress the formation of large holes. The former mechanism is the most important, which is illustrated by the fact that diffusion of OH has little influence on the voltammetry for $D_{\mathrm{CO}}=0$, as the CO molecules that are not at the perimeter of the holes can still not react if CO does not diffuse. Even though no large holes are formed when CO diffuses, the number of free sites on the surface is much higher than without CO diffusion, as illustrated in Fig. 2, which shows the various coverages during the positive-going potential sweep. As is clear from the observed responses, poor mixing leads to a relatively broad peak in the voltammogram, whereas high CO diffusion rates lead to the sharp and narrow peaks predicted by the mean-field approximation. We note also that the broad peak for $D=0$ is essentially independent of the CO oxidation rate; even for very fast CO oxidation rates, the voltammetric peak is still broad and not sharply peaked.

Figure 3 shows snapshots of the catalyst surface at various potentials during the sweep. It is clearly seen that for $D=0$ the CO is oxidized only at the rim of a few holes. Note that, since the CO oxidation rate is higher than the OH adsorption rate, the holes are mostly empty in the potential range of the oxidation peak. Only after the CO has been oxidized and the potential is raised further, the surface gets fully occupied by OH. In contrast to the $D=0$ case, for $D=100$ no significant formation of large holes is observed.

For the lower initial coverages of CO [Figs. 1(b) and 1(c)], there are more free sites for the OH adsorption to start and fewer CO molecules exist that can be oxidized only by the growing of existing holes (if CO would not diffuse). Hence, the CO oxidation peak shifts to lower potentials and $D=0$ voltammogram starts resembling the $D=100$ and the mean-field voltammogram. Also note that the H_2O oxidation and OH reduction peaks coincide exactly with the mean-field approximation, as this is a monomolecular surface reaction. Hence, no MC simulation of the return scan of the cyclic voltammogram was carried out.

It is common practice in linear sweep or cyclic voltammetry experiments to determine the potential, E_p, at which the current exhibits a peak, as a function of the scan rate v. For the simple irreversible oxidation (or reduction) of an adsorbed species, this species being the only one present on the surface, a plot of E_p vs $\log v$ yields a slope of 2.3 $k_BT/\alpha e_0 \approx 119$ mV for $T=300$ K and $\alpha=0.5$.[27] For the Langmuir–Hinshelwood-type of mechanism Eqs. (2.1) and (2.2), this rule no longer applies. As an exact analytical derivation of the peak potential of Eqs. (2.1) and (2.2) is not possible (but see Sec. III C), we have plotted the numerically calculated peak potential vs $\log v$ in Fig. 4 for both mean field and $D=0$. The plot is curved in a similar way for the two cases, and a slope of 119 mV is observed only for the highest scan rates. For the lowest scan rates, both mean field and $D=0$ predict a slope of $\sim$40 mV. Palaikis *et al.*[5] have reported slopes of the E_p vs $\log v$ plots for the CO oxidation on Pt(100) and Pt(111) of 60 ± 3 and 80 ± 5 mV, respectively, Richarz[30] reports a slope of $\sim$70 mV for the CO oxidation on polycrystalline Pt. However, these slopes were determined in the relatively narrow scan rate range 5–100 mV s^{-1}, exactly the range where the plot is not expected to be linear according to both our simulations. In fact, if a few theoretical data points in this range are subjected to a linear fit, slopes of $\sim$60–80 mV are obtained. Richarz[30] mentions that deviations from a straight line are found at higher scan rates, and from the few experimental data given by him we deduce that the slope indeed becomes steeper. An analytical derivation of the slopes at low and high v will be given in Sec. III C.

Experimentally, the CO oxidation peak on Pt(100) is sharp and would resemble the mean-field voltammogram in Fig. 1(a), suggesting that CO diffuses quickly on the Pt surface. However, ''sharpness'' is a rather subjective quality that depends on the scales of the axes. A more quantitative test is desirable. Potential step experiments, as described in the next section, could provide such a test.

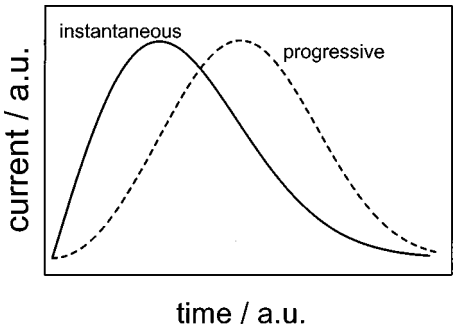

FIG. 6. Current transients for instantaneous and progressive nucleation and growth.

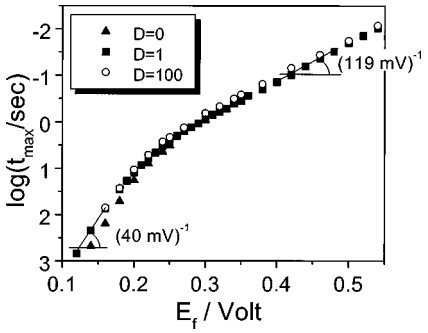

FIG. 7. The logarithm of the time of the current maximum as a function of the final potential.

B. Potential step chronoamperometry of FAST

Potential step experiments provide the best way to study electrochemical reactions that proceed through the nucleation and growth of reactive islands. McCallum and Pletcher[2] have studied the CO oxidation on polycrystalline Pt by potential step experiments, and Love and Lipkowski[7] have repeated these experiments for single-crystal electrodes. MC simulations of potential step transients of a model similar to ours were recently reported by Petukhov.[31]

Figure 5 shows the current transients obtained by stepping from a potential at which a $\theta_{CO}^{i}=0.99$ CO submonolayer is stable, to four different final potentials E_f. The transients as predicted by the mean-field equations are also given (dashed lines). At the most positive final potential [Fig. 5(a)], the transient is not very sensitive to the CO diffusion rate. The curves for $D=0$ and $D=100$ are indistinguishable, though both deviate strongly from the mean-field transient. This is understandable as at such positive potentials, practically all the holes in the CO layer and empty sites are filled up immediately by OH, leaving no room for CO surface migration. At less positive final potentials [Fig. 5(b)], we start observing differences in the current transients. There are apparently enough vacant surface sites to allow CO diffusion to have an influence on the chronoamperometric response. For a potential at the foot of the voltammetric oxidation peak in Fig. 1(a), the qualitative shape of the transients is significantly different, as shown in Fig. 5(c). The transient for fast diffusion ($D=100$) rises much faster than for $D=0$, and collapses very rapidly after having reached its maximum current. This transient is now quite close to the mean-field transient. For extremely low final potential E_f [Fig. 5(d)], even a slow diffusion $D=1$ gives a transient markedly different from the $D=0$ transient, though the fast decay after the current maximum, as in Fig. 5(c), no longer occurs. We note also that the asymmetric transients for mean field in Figs. 5(a) and 5(b) and for mean field and $D=100$ in Fig. 5(c) were not found by other authors who carried out a potential step analysis of a Langmuir–Hinshelwood mechanism very similar to ours.[30,31]

The origin of the shape of the transients and the difference between the two transients for slow and fast surface diffusion can be understood, at least qualitatively, by discussing the classical theory for the nucleation and growth of two-dimensional films.[28,32] Let M_0 be the number of holes in the initial CO layer. In the case of a so-called instantaneous nucleation, these holes are occupied instantaneously. If the nucleus grows at a rate k_G, the total ''extended'' area covered by M_0 *nonoverlapping* islands is

$$S_{ex}^{inst} \propto M_0 k_G^2 t^2. \tag{3.1}$$

In the case of progressive nucleation, the nucleation rate is so low that $k_N t \ll 1$ such that the number of nuclei grows linearly in time, $M(t)=k_N M_0 t$, where k_N is the nucleation rate constant. The extended area now scales with the third power of the elapsed time

$$S_{ex}^{prog} \propto M_0 k_N k_G^2 t^3. \tag{3.2}$$

At longer times, islands start to coalesce. In the case that the nuclei are distributed randomly over the surface, the area S that is actually covered by the coalescing islands is related to the extended area by Avrami's theorem,[33]

$$S=1-\exp(-S_{ex}). \tag{3.3}$$

Avrami's theorem holds for islands of equal sizes as well as for islands of unequal sizes. Note that we consider unit area; in the general case, S and S_{ex} are in fact fractional coverages θ and θ_{ex} (where θ_{ex} may exceed 1). The concomitant current transient is obtained by

$$i(t) \propto \frac{d\theta}{dt}. \tag{3.4}$$

This leads to well-known expressions for the current transients in the cases of instantaneous and progressive nucleation, first derived by Bewick, Fleischmann, and Thirsk (BFT).[32] For instantaneous nucleation, one finds:

$$i(t) \propto M_0 k_G^2 t \ \exp(-\pi M_0 k_G^2 t^2), \tag{3.5}$$

and for progressive nucleation:

$$i(t) \propto M_0 k_N k_G^2 t^2 \ \exp(-\pi M_0 k_N k_G^2 t^3/3). \tag{3.6}$$

These transients are illustrated in Fig. 6. We find that the equation for progressive nucleation fits quite well the MC transients of FAST for slow CO diffusion. This is understandable as the OH formation reaction is slower than the CO oxidation reaction for all potentials, and hence an instantaneous nucleation mechanism could not apply. The reason why deviations from the BFT theory are observed for fast CO diffusion as in Fig. 5(c) lies in a breakdown of the Avrami theorem. For $E_f=0.275$ V, the ''islands'' consist of

mainly empty sites with ~10% OH, and hence the CO can diffuse into the existing islands and react. This case, i.e., reaction occurring on already existing islands, is prohibited in the derivation of the Avrami theorem. This effect causes a higher peak current in the transient, and a faster decay after the current maximum, as observed in Fig. 5(c). For very low final potentials, such as in Fig. 5(d), CO can only be oxidized if an OH happens to adsorb next to it, since the equilibrium coverage by OH at these low potentials is essentially zero. Finally, we note that if OH diffuses with $D_{OH}=100$, and $D_{CO}=0$, the transient in Fig. 5(c) does not change appreciably with respect to $D_{OH}=0$: the current maximum shifts to a slightly lower time (1.4 s), but the shape of the transient remains the same.

Experimentally, Love and Lipkowski[7] have found that, at low final potentials, the transients are well described by the BFT theory for progressive nucleation, with an initial quadratic rise in current, as in our model simulation for low CO diffusion rates. For higher final potential, the shape of the experimental transients of Love and Lipkowski changes into the one typical for an instantaneous nucleation mechanism, with an initial linear rise in current (Fig. 6). Such behavior is not observed in our simulations.

As the inverse of the time corresponding to the current maximum can be taken as a measure of the reaction rate, Love and Lipkowski have plotted the logarithm of the time of the current maximum against the final potential E_f. In Fig. 7, we present such a Tafel plot obtained from our simulations. Two different slopes, at high and low final potential, are observed. This change in slope is also observed experimentally. Note that these slopes do not depend on the surface diffusion rate D. For low E_f, the slope is ca. $(40\ \mathrm{mV})^{-1}$; for high E_f, the slope is ca. $(119\ \mathrm{mV})^{-1}$. The experimental slopes obtained by Love and Lipkowski for Pt(100), Pt(311) and Pt(111) seem to be approximately twice as small, i.e., $(80\ \mathrm{mV})^{-1}$ and $(240\ \mathrm{mV})^{-1}$, resp. A similar discrepancy with experiment is observed for the SLOW set of rate constants; a discussion of the possible origin of this difference will be postponed to Sec. III E.

The values of the slopes at low and high final potential can be understood by having a closer look at the Langmuir-Hinshelwood mechanism Eqs. (2.1) and (2.2). First, for a progressive nucleation and growth transient, the time corresponding to the current maximum is given by

$$t_{\max}=\left(\frac{2}{\pi k_N k_G^2}\right)^{1/3} \tag{3.7}$$

and hence the slope is

$$-\frac{d\ \log\ t_{\max}}{dE}=\frac{1}{3}\frac{d\ \log\ k_N}{dE}+\frac{2}{3}\frac{d\ \log\ k_G}{dE}. \tag{3.8}$$

For very high final potentials, the OH desorption is negligible both with respect to the OH adsorption and the CO +OH oxidation reaction, so that effectively $k_G \approx k_N$. The nucleation rate constant is simply the rate of OH adsorption v_1, whose potential dependence predicts a slope of $2.3k_BT/\alpha e_0=119$ mV, in agreement with the simulation. For very low final potentials, the OH desorption is much faster

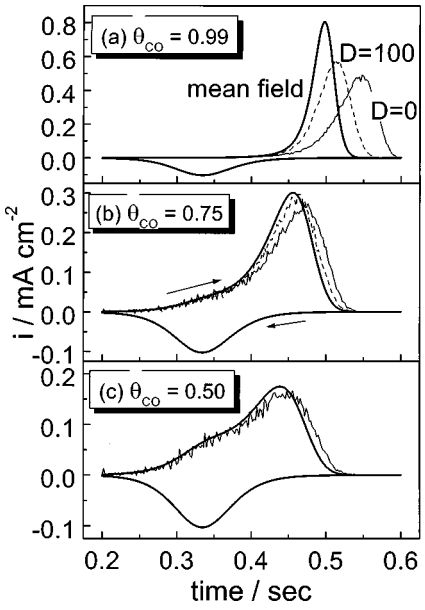

FIG. 8. Cyclic voltammograms for the SLOW set of rate constants at three different initial coverages of CO, as indicated in the figure. The sweep rate is 50 mV s^{-1}. Thick solid line, mean field; thin dashed line, $D=100$; thin solid line, $D=0$.

than the CO+OH reaction. Hence we can treat the OH adsorption/desorption reaction as being in quasiequilibrium, that is,

$$\theta_{OH}^{eq}=\frac{k_{ads,OH}(1-\theta_{CO})}{k_{ads,OH}+k_{des,OH}+k_{CO_2,des}\theta_{CO}}$$

$$\approx\frac{k_1}{k_{-1}}\ \exp\left(\frac{e_0E}{k_BT}\right)(1-\theta_{CO}). \tag{3.9}$$

The nucleation rate is now

$$k_N=v_1\approx k_{ads,OH}(1-\theta_{OH}^{eq}-\theta_{CO})$$

$$=\frac{k_1^2}{k_{-1}}\ \exp\left(\frac{(1+\alpha)e_0E}{k_BT}\right) \tag{3.10}$$

and the growth rate is

$$k_G=v_2=k_{des,CO_2}\theta_{OH}^{eq}\theta_{CO}$$

$$\approx\frac{Zk_2k_1}{k_{-1}}\theta_{CO}(1-\theta_{CO})\ \exp\left(\frac{(1+\alpha)e_0E}{k_BT}\right). \tag{3.11}$$

Both predict a slope of $2.3\ k_BT/(1+\alpha)e_0\approx 40$ mV, and hence from Eq. (3.8) a slope of 40 mV is expected, in agreement with the simulation results.

Results completely similar to those shown in Fig. 7 are obtained if instead of the logarithm of the current maximum, the logarithm of the slope of the initial part of the i vs t^2 transient [or, more precisely, the $(\mathrm{slope})^{1/3}$] is plotted vs the final potential.

From the above, we conclude that the change in slope observed in Fig. 7, that is also observed experimentally, is *not* due to a change in nucleation-and-growth mechanism, i.e., from a progressive at low to an instantaneous nucleation-and-growth mechanism at high potentials. This

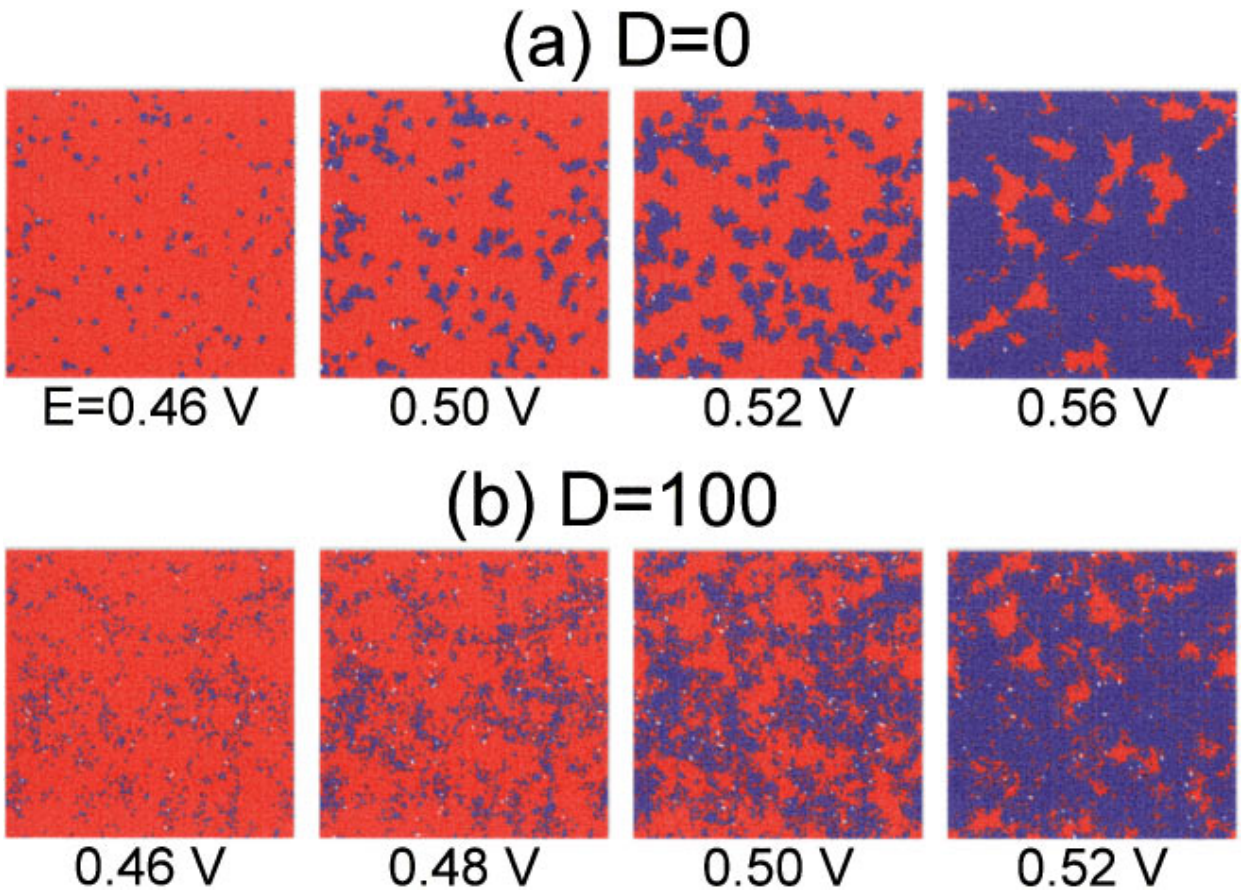

FIG. 9. Snapshots of the electrode surface during the voltammograms of Fig. 8(a). Blue, OH; Red, CO; White, empty site.

has been implied by Love and Lipkowski, who indeed also observed a change in the shape of the current transient as a function of the final potential. However, the nucleation-and-growth mechanism is progressive for all potentials plotted in Fig. 7, and the transients have the corresponding shape. A similar result holds for the instantaneous nucleation-and-growth mechanism, as will be shown in Sec. III D. In the model, the change in slope is caused by the multistep character of reaction mechanism, in particular through the desorption reaction; OH desorption does not play a role at high potentials, whereas it plays a non-negligible role at low potentials.

C. Cyclic voltammetry of SLOW

In Fig. 8 we show the voltammetric results (at 50 mV s^{-1}) obtained with the rate constants given in the SLOW column of Table I, for three different initial CO coverages. Because the CO+OH reaction is now slow with respect to the OH adsorption, the CO oxidation peak occurs at a potential more positive than the OH adsorption/desorption peaks. Again it is seen that the deviations from the mean-field approximation are the most significant for high initial CO coverage. In contrast to the FAST voltammetry, there are very few empty sites on the surface. Therefore it is more difficult to suppress island formation, even for $D=100$, as can be seen in Fig. 9, which shows snapshots of the surface during the CO oxidation peak of Fig. 8(a).

In Fig. 10 the peak potential E_p is plotted as a function of $\log v$. Again a nonlinear plot is obtained, which changes slope from 40 mV at low v to 119 mV at high v. A simple explanation to understand this feature follows the arguments of the previous section. At low v, the peak potential occurs in a potential region where OH desorption is the fastest reaction and hence OH can be considered in a kind of quasi-equilibrium. The CO oxidation rate is then governed by Eq. (3.11). At high v, the peak potential occurs in a potential region where OH desorption can be neglected and the OH adsorption is the fastest process. As can be seen from the snapshots in Fig. 9, in this potential region $\theta_{OH} \approx 1-\theta_{CO}$ and

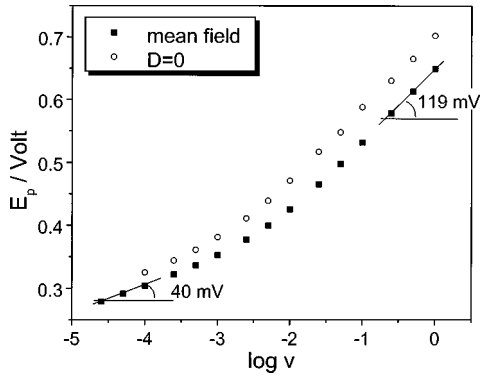

FIG. 10. Peak potential E_p as a function of the logarithm of the sweep rate v.

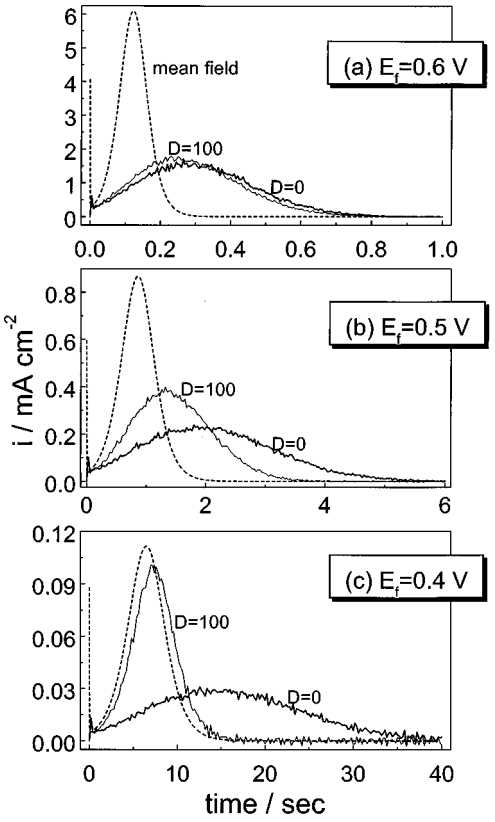

FIG. 11. Potential step current transients for the SLOW set of rate constants from a 0.99 CO monolayer to three different final potentials E_f, as indicated in the figure.

hence the rate of CO oxidation is, in the mean-field approximation

$$\frac{d\theta_{\mathrm{CO}}}{dt} = -Zk_2\theta_{\mathrm{CO}}(1-\theta_{\mathrm{CO}})\exp(\alpha e_0 E(t)/k_BT). \quad (3.12)$$

Equations (3.11) and (3.12) have exactly the same structure, apart from the different proportionality constant in the exponential term. Given that $E(t)=E_i+vt$, and $\theta_{\mathrm{CO}}(t=0)=\theta^i_{\mathrm{CO}}$, the solution of this differential equation reads

$$\theta_{\mathrm{CO}}(t)=\frac{\Theta(E(t))}{1+\Theta(E(t))}, \quad (3.13)$$

where for Eq. (3.12) the Θ function is given by

$$\Theta(E(t)) = \exp\left(-\frac{Zk_2k_BT}{\alpha e_0 v}\exp(\alpha e_0 E(t)/k_BT) + \frac{Zk_2k_BT}{\alpha e_0 v}\exp(\alpha e_0 E_i/k_BT) + \ln\frac{\theta^i_{\mathrm{CO}}}{1-\theta^i_{\mathrm{CO}}}\right)$$
$$= \exp(f(E(t))-f(E_i)+C_0). \quad (3.14)$$

For Eq. (3.11) one simply replaces α by $(1+\alpha)$. At high v, the CO oxidation current is given by

$$i = i_0\theta_{\mathrm{CO}}(1-\theta_{\mathrm{CO}})\exp(\alpha e_0 E/k_BT). \quad (3.15)$$

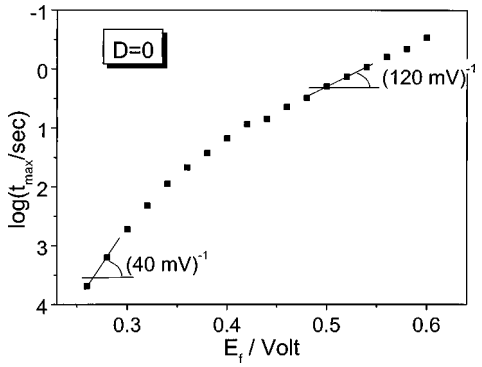

FIG. 12. The logarithm of the time of the current maximum as a function of the final potential.

Taking the derivative of this expression with respect to E, and realizing that θ_{CO} depends on E according to Eq. (3.13), one finds the following expression for the peak potential:

$$f(E_p)=\frac{1+\exp(f(E_p)-f(E_i)+C_0)}{\exp(f(E_p)-f(E_i)+C_0)-1}. \quad (3.16)$$

For low v, one again replaces α by $(1+\alpha)$ in Eqs. (3.15) and (3.16). A physically acceptable solution of this problem is one in which E_p does not depend on the starting potential E_i such that we can put $f(E_i)=0$. This condition is satisfied only if $(Zk_2k_BT/\alpha e_0 v)\to 0$, i.e., if the irreversible reaction is very slow or the scan rate very high. To obtain the desired relationship between E_p and $\log v$, we are looking for a solution of the kind

$$f(E_p)=A, \quad (3.17)$$

where A is some constant which depends only on θ^i_{CO}. One can verify numerically that A indeed exists (for $\theta^i_{\mathrm{CO}}=0.99$, $A\approx -5.00$), and hence Eq. (3.17) is a solution of Eq. (3.16). Rearranging Eq. (3.17) gives

$$E_p = 2.3\frac{k_BT}{\alpha e_0}\log v + C \quad (3.18)$$

at high v, and

$$E_p = 2.3\frac{k_BT}{(1+\alpha)e_0}\log v + C' \quad (3.19)$$

at low v, where C and C' are constants that are of no concern to us. Hence, for high v, the slope is expected to be $2.3k_BT/\alpha e_0 \approx 119$ mV, and for low v $2.3k_BT/(1+\alpha)e_0 \approx 40$ mV. However, it has to be remembered that the above arguments only apply if the irreversible reaction is very slow or the scan rate very high. Indeed, in our calculations presented in Sec. III A (Fig. 4), in which the irreversible reaction is relatively fast, we found that for the lowest scan rates, E_p starts showing a dependence on E_i and the 40 mV slope is not found for scan rates lower than the ones shown in Fig. 4.

D. Potential step chronoamperometry of SLOW

Figure 11 shows three potential step transients for an initial CO coverage of 0.99. For $D=0$, the transients correspond approximately to an instantaneous nucleation mecha-

nism. However, for low E_f and high diffusion rates, we obtain a transient with a much clearer initial quadratic rise in current, as shown in Fig. 11(c). Under these conditions, the high CO diffusion rate causes an enhancement of the growth rate of the OH islands due to the improved mixing.[31] Note that, in contrast to the transient in Fig. 5(c), the transient in Fig. 11(c) does not deviate from the shape predicted by the BFT theory. The reason for this is the lack of a sufficiently high number of empty sites. Recall that for the FAST set of rate constants, the islands mainly consist of empty sites, and CO can diffuse into these islands, which causes a breakdown of the Avrami theorem. For the SLOW set of rate constants, the islands consist mainly of OH, and the islands coalesce in accordance with the Avrami theorem. For $D=100$, we observe a transition from a progressive nucleation-and-growth mechanism at low to an instantaneous nucleation-and-growth mechanism at high final potentials. The transition is also observed for somewhat lower diffusion rates, such as $D=10$. This is exactly the transition observed experimentally by McCallum and Pletcher[2] and Love and Lipkowski.[7] It is quite interesting to note that we cannot explain this transition, with the present model, without invoking the role of CO diffusion.

The logarithm of the time of the current maximum is plotted vs the final potential in Fig. 12. The by now familiar change in slope from 40 to 119 mV is observed. According to the BFT theory,

$$t_{\max}=\left(\frac{1}{2\pi M_0 k_G}\right)^{1/2}, \tag{3.20}$$

and hence the plot has a slope of $d\log k_G/dE$. Again the arguments of previous sections can be used to explain the different slopes at low and high E_f.

E. Comparison of FAST and SLOW with experiment

In this section, we discuss more specifically the differences between the FAST and SLOW sets of rate constants and how the simulations relate to experimental results.

One conspicuous difference between the voltammetry of FAST and SLOW is the fact that, for FAST, the CO oxidation peak occurs at a potential negative with respect to the OH adsorption-desorption peaks in CO-free solution (Fig. 1), whereas for SLOW, the CO oxidation peak occurs more positive than the OH adsorption-desorption peaks (Fig. 8). Another consequence of this difference in CO oxidation rates is that the total charge associated with the CO oxidation peak corresponds to 2 electrons per site for FAST, and to 3 electrons per site for SLOW, as in the latter case completion of the CO oxidation leads to a surface fully covered by OH. Interestingly, these facts agree very well with the different situations for CO oxidation on Pt and Rh single crystals. On Pt(111) and Pt(100), the voltammetry in perchloric acid is very similar to our Fig. 1(a) with fast CO diffusion, i.e., very sharply peaked (see, e.g., Fig. 2 in Ref. 12 and Figs. 4 and 5 in Ref. 5); assuming the CO oxidation requires 2 electrons, the coverage estimated from the peak area agrees quite well with more direct spectroscopic estimates. On the other hand, the voltammetry on Rh(100) is comparable to that shown in Fig. 8(a) (i.e., mean field and $D=100$), with similar positions of the CO oxidation and the OH reduction peaks.[34] The coverage estimated from the peak area is indeed about 1.5 times higher than that obtained from infrared measurements. This indicates that on rhodium the dissociative water adsorption reaction (2.1) has its equilibrium on the OH side after the CO oxidation has been completed, implying that CO oxidation is much slower than OH adsorption. This would agree with recent *ab initio* quantum-chemical calculations which indicate that OH binds more strongly to Rh than to Pt, and is hence more reactive on Pt.[35]

If CO diffusion on Pt is fast, as one would conclude from a comparison of the experimental and simulated voltammetry, our model would predict deviations from the classical BFT current transients in potential step experiments, a typical example of which is shown in Fig. 5(c). Such deviations have not been reported by Love and Lipkowski.[7] However, depending on the exact CO surface mobility, these deviations may occur in only a limited range of final potentials. For rhodium, we are not aware of any potential step experiments, though such experiments would be interesting for comparison with platinum.

Some authors have suggested that the fact that the CO oxidation peak occurs well before the OH adsorption peak in a CO-free solution, implies that the oxygen-containing species reacting with adsorbed CO must be adsorbed H_2O rather than adsorbed OH. Our calculations clearly illustrate that if the CO+OH reaction is fast, only a low OH coverage is needed to oxidize a CO monolayer. In Fig. 2(a), the OH coverage after the completion of the CO oxidation is about 0.10 and would be even lower for higher CO oxidation rates.

Finally, we return to the discrepancy between the experimental Tafel slopes and the ones predicted by our model. As was already mentioned in Sec. III B, the experimental slopes reported by Love and Lipkowski deviate by a factor of 2 from the theoretical slopes, i.e., 80 and 240 mV, instead of 40 and 120 mV as predicted by our model. If this deviation is real, one should also observe it in the $E_p-\log v$ plots. Only Palaikis *et al.*[5] and Richarz[30] have reported such measurements, unfortunately only at relatively low scan rates, and found slopes of 60–80 mV. Especially the slope of 60 mV is inconsistent with the slopes reported by Love and Lipkowski, and we believe that the explanation given in Sec. III A, namely, that the 60–80 mV slopes were measured in the transition region of Fig. 4, is quite a plausible one. The only major difference in experimental conditions between the measurements of Love and Lipkowski and Palaikis *et al.*, is the different base electrolyte concentration. Palaikis *et al.* worked in a 1 M $HClO_4$ solution, whereas Love and Lipkowski used a 0.1 M $HClO_4$ solution. This could point towards a double-layer effect, as in the experiments of Love and Lipkowksi the double layer is more extended and hence the differences in the electrostatic potential that are experienced by species absorbed onto the electrode are only some fraction of the difference in the externally applied potential. If for instance the adsorbed OH is only partially discharged (as seems to be the case for OH adsorbed on gold[36]), the extension of the double layer would have a strong influence on the electrosorption valence.[28] An electrosorption valence

different from 1 would change the potential dependence of Eqs. (2.3)–(2.5). Clearly this explanation can only be tentative and awaits further experimental investigation.

IV. CONCLUSIONS AND SUMMARY

In this paper we have presented a detailed analysis of a simple, but commonly accepted model of the electrocatalytic CO oxidation on a platinum electrode. Although the model treats the structural features of the real system in a far too simplified manner, for the first time we have been able to obtain quite a detailed picture of the role of CO surface mobility on the macroscopic electrochemical response by making use of an efficient Monte Carlo algorithm which allows the exact introduction of time in the MC methodology. This is in fact the first application of this DMC method to an electrocatalytic reaction. The principal result of the paper is that the mean-field approximation, which is the standard (though often tacitly made) assumption in the electrochemical literature, breaks down severely if the adsorbed species which are involved in bimolecular surface reactions, do not diffuse. This result is well established in the statistical mechanics literature,[24] but it seems to be especially relevant to electrochemistry as many authors have invoked from their measurements that CO has a low mobility at the Pt/solution interface at room temperature.[9,10] This situation is in contrast with the CO oxidation on the Pt/gas interface, for which CO mobility is known to be high.[37]

Our MC results do not directly lend support to the idea that CO mobility is low at the platinum/solution interface. The experimental voltammetric peak on Pt(100) and Pt(111) is very sharp, which can only be reproduced by our simulations if CO diffusion is fast. However, if the CO+OH reaction is assumed to be the intrinsically fastest reaction on the surface, and CO mobility is high, as seems to be the case for platinum, interesting deviations from the classical BFT theory for potential step current transients would be expected due to a breakdown of the Avrami theorem. Such deviations have not yet been reported experimentally.[7] Experimentally, there is a transition from a progressive nucleation and growth at low potential to an instantaneous nucleation and growth mechanism at high final potentials. This trend is also not exactly reproduced by our MC simulations. However, it may be that at higher final potentials additional surface reactions take place that are not included in our simple model. At any rate, our results show clearly the type of information that can be obtained from detailed MC and mean-field simulations of an assumed reaction mechanism, especially in direct comparison with experimental results.

The nonlinear plot of $\log t_{\max}$ vs E_f observed by Love and Lipkowski in their potential step experiments is evidence for the correctness of the Langmuir-Hinshelwood mechanism for the electrocatalytic CO oxidation as summarized in Eqs. (2.1) and (2.2). However, the nonlinearity of the plot is not due to a change in nucleation-and-growth mechanism, as has been suggested by these authors, but rather to the influence of the OH desorption reaction which changes with potential. In fact, we have shown that a very similar result should be obtained from a plot of the voltammetric peak potential vs the logarithm of the scan rate, a remarkably simple prediction that apparently has not been realized before in the literature and awaits experimental confirmation. We believe that since the change in the theoretical slopes agrees well with the experimental changes (even though their absolute values differ by a factor of 2, an admittedly somewhat disturbing discrepancy which also deserves further experimental study), we have provided evidence that the oxygen-containing species with which CO reacts on the surface, is an OH species and not an adsorbed H_2O species, as has been suggested by some authors. The rate of formation of such a H_2O species would be expected to have a much too weak potential dependence to explain the experimentally observed trends.

We think that the methodology presented in this paper, in spite of the still quite high level of simplicity, holds great promise in the understanding of electrocatalytic activity. There are many avenues open for future research. On the theoretical side, it is of interest to develop approximations that go beyond the mean-field approximation and compare them to the MC results.[24] Also, the reaction model itself could be refined. One possibility is to treat more accurately the structural details of the CO adsorption, by allowing for adsorption on bridge and other multicoordinated sites, and including lateral interactions. It is known that the small prewave which is observed in the oxidation of CO from a Pt(111) electrode, is due to the oxidation of multicoordinated CO.[14] The main oxidation wave is due to the oxidation of linearly and bridge-bonded CO. The CARLOS program was in fact designed to allow for multiple types of adsorption. Another interesting topic is CO oxidation on modified Pt electrodes, such as Pt/Ru, Pt/Bi or Pt/Sn electrodes.[15,38–40] One expects the activity of such substrates to depend quite critically on the CO migration properties, especially if the foreign metal forms islands on the surface. Finally, more complex reactions can be studied, such as methanol or formic acid oxidation.

ACKNOWLEDGMENT

The research of M.T.M.K. was supported by a fellowship from the Royal Netherlands Academy of Arts and Sciences (KNAW).

[1] S. Gilman, J. Phys. Chem. **68**, 70 (1964).
[2] C. McCallum and D. Pletcher, J. Electroanal. Chem. **70**, 277 (1978).
[3] B. Beden, S. Bilmes, C. Lamy, and J. M. Léger, J. Electroanal. Chem. **149**, 295 (1983).
[4] E. Santos, E. P. M. Leiva, W. Vielstich, and U. Linke, J. Electroanal. Chem. **227**, 199 (1987).
[5] L. Palaikis, D. Zurawski, M. Hourani, and A. Wieckowski, Surf. Sci. **199**, 183 (1988).
[6] F. T. Wagner and T. E. Moylan, ACS Symp. Ser. **378**, 65 (1988).
[7] B. Love and J. Lipkowski, ACS Symp. Ser. **378**, 484 (1988).
[8] B. Beden, C. Lamy, N. R. de Tacconi, and A. J. Arvia, Electrochim. Acta **35**, 691 (1990).
[9] A. M. de Becdelièvre, J. de Becdelièvre, and J. Clavilier, J. Electroanal. Chem. **294**, 97 (1990).
[10] J. M. Feliu, J. M. Orts, A. Fernandez-Vega, A. Aldaz, and J. Clavilier, J. Electroanal. Chem. **296**, 191 (1990).
[11] D. Zurawski, M. Wasberg, and A. Wieckowksi, J. Phys. Chem. **94**, 2076 (1990).
[12] M. J. Weaver, S.-C. Chang, L.-W. Leung, X. Jiang, M. Rubel, M. Szklarczyk, D. Zurawski, and A. Wieckowski, J. Electroanal. Chem. **327**, 247 (1992).

[13] J. A. Caram and C. Gutiérrez, J. Electroanal. Chem. **346**, 451 (1993).
[14] I. Villegas and M. J. Weaver, J. Chem. Phys. **101**, 1648 (1994).
[15] H. A. Gasteiger, N. Markovic, P. N. Ross, Jr., and E. J. Cairns, J. Phys. Chem. **98**, 617 (1994).
[16] P. A. Rikvold, J. Zhang, Y.-E. Sung, and A. Wieckowski, Electrochim. Acta **41**, 2175 (1996).
[17] G. Brown, P. A. Rikvold, M. A. Novotny, and A. Wieckowksi, Electrochim. Acta (preprint).
[18] M. T. M. Koper, J. Electroanal. Chem. **450**, 189 (1998).
[19] D. A. Harrington, J. Electroanal. Chem. **420**, 101 (1997).
[20] A. P. J. Jansen, Comput. Phys. Commun. **86**, 1 (1995).
[21] R. Imbihl and G. Ertl, Chem. Rev. **95**, 697 (1995).
[22] E. M. Patrito, P. P. Oliviera, and H. L. Sellers, Surf. Sci. **306**, 447 (1994).
[23] A. Fahmi and R. A. van Santen, Z. Phys. Chem. **197**, 203 (1997).
[24] R. M. Nieminen and A. P. J. Jansen, Appl. Catal., A **160**, 99 (1997).
[25] CARLOS is developed and implemented by Dr. J. J. Lukkien of the Department of Computing Science, Eindhoven University of Technology, The Netherlands; J. J. Lukkien, J. P. L. Segers, P. A. J. Hilbers, R. J. Gelten, and A. P. J. Jansen, Phys. Rev. E **58**, 2598 (1998).
[26] R. J. Gelten, A. P. J. Jansen, R. A. van Santen, J. J. Lukkien, J. P. L. Segers, and P. A. J. Hilbers, J. Chem. Phys. **108**, 5921 (1998).
[27] See, e.g., P. A. Christensen and A. Hamnett, *Techniques and Mechanisms in Electrochemistry* (Blackie, London, 1994), p. 61.
[28] W. Schmickler, *Interfacial Electrochemistry* (Oxford University Press, New York, 1996).
[29] E. G. Seebauer and C. E. Allen, Prog. Surf. Sci. **49**, 265 (1995).
[30] F. Richarz, *Elektrochemisch Erzeugte Pt, Ru und PtRu-Elektroden: Charakterisierung und Elektrooxidation von Kohlenmonoxid* (VDI, Düsseldorf, 1995).
[31] A. V. Petukhov, Chem. Phys. Lett. **277**, 539 (1997).
[32] A. Bewick, M. Fleischmann, and H. R. Thirsk, Trans. Faraday Soc. **58**, 2200 (1962).
[33] M. Avrami, J. Chem. Phys. **7**, 1103 (1939); **8**, 212 (1940); **9**, 177 (1941).
[34] S.-C. Chang, Y. Ho, and M. J. Weaver, J. Electrochem. Soc. **139**, 147 (1992).
[35] M. Chen, S. P. Bates, R. A. van Santen, and C. M. Friend, J. Phys. Chem. B **101**, 10051 (1997).
[36] J. Lipkowksi (personal communication).
[37] C. T. Campbell, G. Ertl, H. Kuipers, and J. Segner, J. Chem. Phys. **73**, 5862 (1980).
[38] M. Watanabe and S. Motoo, J. Electroanal. Chem. **60**, 295 (1975).
[39] K. A. Friedrich, K.-P. Geyzers, U. Linke, U. Stimming, and J. Stumper, J. Electroanal. Chem. **402**, 123 (1996).
[40] B. E. Hayden, A. J. Murray, R. Parsons, and D. J. Pegg, J. Electroanal. Chem. **409**, 51 (1996).